Properties of LAr

All values are on the liquid-vapor saturation line and at E=500 V/cm unless otherwise indicated.

Quantity	Symbol	Value	Units	Comments or [Ref]
Atomic number	Z	18		
Atomic weight	A	39.948(1)	g/mol	
Isotopic composition	A=36, 38, 40 stable; 39, 42 $t_{1/2}$>1y			[1, 2,3]
Thermodynamic properties				
Normal boiling point	T_{NBP}	87.303(2)	K	[4]
Density	ρ_{NBP}	1.396(1)	g/ml	[4]
Vapor/liquid volume ratio	V(g)/V(l)	241.7	none	At T_{NBP} [5]
Normal freezing point	T_{FUS}	83.8(3)	K	[4]
Temperature at triple point	T_{TRIPLE}	83.8058	K	ITS-90 def. [4]
Pressure at triple point	P_{TRIPLE}	0.68891(2)	bar	[4]
Density at triple point	ρ_{TRIPLE}	1.417	g/ cm^3	[5]
Temperature at critical point	T_C	150.687(15)	K	[4]
Pressure at critical point	P_C	48.63(3)	bar	[4]
Density at critical point	ρ_C	0.5356(10)	g/ cm^3	[4]
Heat of vaporization	ΔH_{VAP}	161.14	kJ/kg	[5]
Heat capacity	C_P	1.117	kJ/kg/K	[5]
Thermal conductivity	K	0.1256	W/m/K	[5]
Viscosity	η	270.7	μPa s	[5]
Speed of sound	v_S	838.3(1)	m/s	[5]
Response to electromagnetic radiation				
Dielectric constant	ε	1.505(3)		[6,7]
Index of refraction	n	1.38		At 128 nm [8,9,10]
Rayleigh scattering length	L_R	95	cm	At 128 nm [11,12,13]
Absorption length	L_A	>200	cm	For λ>128 nm
Response to ionizing radiation				
W-value for ionization	W_I	23.6(3)	eV/pair	mip [14, 15]
W-value for scintillation	W_S	19.5(10)	eV/photon	mip [16]
W-value for Cerenkov radiation	W_C	2700	eV/photon	β=1 [17]
Fano factor	F	0.107	none	[18]
Moliere radius	R_M	10.0	cm	[19]
Radiation length	X_0	14.0	cm	[19]
Nuclear interaction length	λ_I	85.7	cm	[19]
Critical energy	E_C	30.5	MeV	[19]
Minimum specific energy loss	dE_{MIP}/dx	2.12	MeV/cm	[19]
Scintillation emission peak	λ_{SCINT}	128(10)	nm	[20]
Decay time	τ_{SCINT}	6(2), 1590(100)	ns	[21]

Charged particle transport properties				
Electron drift velocity	v_D(e-)	1.60(2)	mm/μs	At T_{NBP} [22-25]
… variation wrt temperature	δLog(v_D)/δT	-1.9	%/K	
… variation wrt field	δLog(v_D)/δE	+0.094	%/(V/cm)	
Electron saturation drift velocity	v_{SAT}(e-)	6.6	mm/μs	[39]
Electron mobility at zero field	μ_0	518(2)	cm^2/V s	At T_{NBP}
Ion drift velocity	v_D(Ion)	$8.0(4)\times10^{-6}$	mm/μs	At T_{NBP} [26]
… variation wrt temperature	δLog(v_D)/δT	+3.5	%/K	
… variation wrt field	δLog(v_D)/δE	+0.2	%/(V/cm)	
Electron transverse diffusion coef.	D_T(e-)	13(2)	cm^2/s	[27,28,29]
Electron longitudinal diffusion coef.	D_L(e-)	5(1)	cm^2/s	[29,30]
Electron diffusion at zero field	D_0	3.9	cm^2/s	At T_{NBP}
Ion diffusion coefficient	D_+	3.2×10^{-3}	cm^2/s	for TE
Recombination constant	R	0.66		For mip [31,32]
Electron attachment rate constant	k_S	2.0×10^{3}	ppb^{-1} s^{-1}	For O_2 [33-37]

Isotopic composition and radiological purity

Isotope	Relative Mass	Abundance[3]	Decay Mode[3]	Half Life[3]	Q-value (MeV)[3]
36	35.967 546 28(27)	0.337(3)	stable	-	-
37		nil	EC, β^+	35.04 d	0.8135(3)
38	37.962 732 2(5)	0.063(1)	stable	-	-
39		1.01(8) Bq/kg [1]	β^-	269 y	0.565(5)
40	39.962 383 123(3)	99.600(3)	stable	-	-
41		nil	β^-	109.34 m	2.4916(7)
42		6×10^{-5} Bq/kg [2]	β^-	32.9 y	0.599(40)

Also ^{85}Kr (β^-, E_β =0.687 MeV, $t_{1/2}$=10.756 y) is a common radioactive contaminant of LAr at the level of 0.1 to 0.3 Bq/kg

Thermodynamic Properties

Phase Diagram [4]

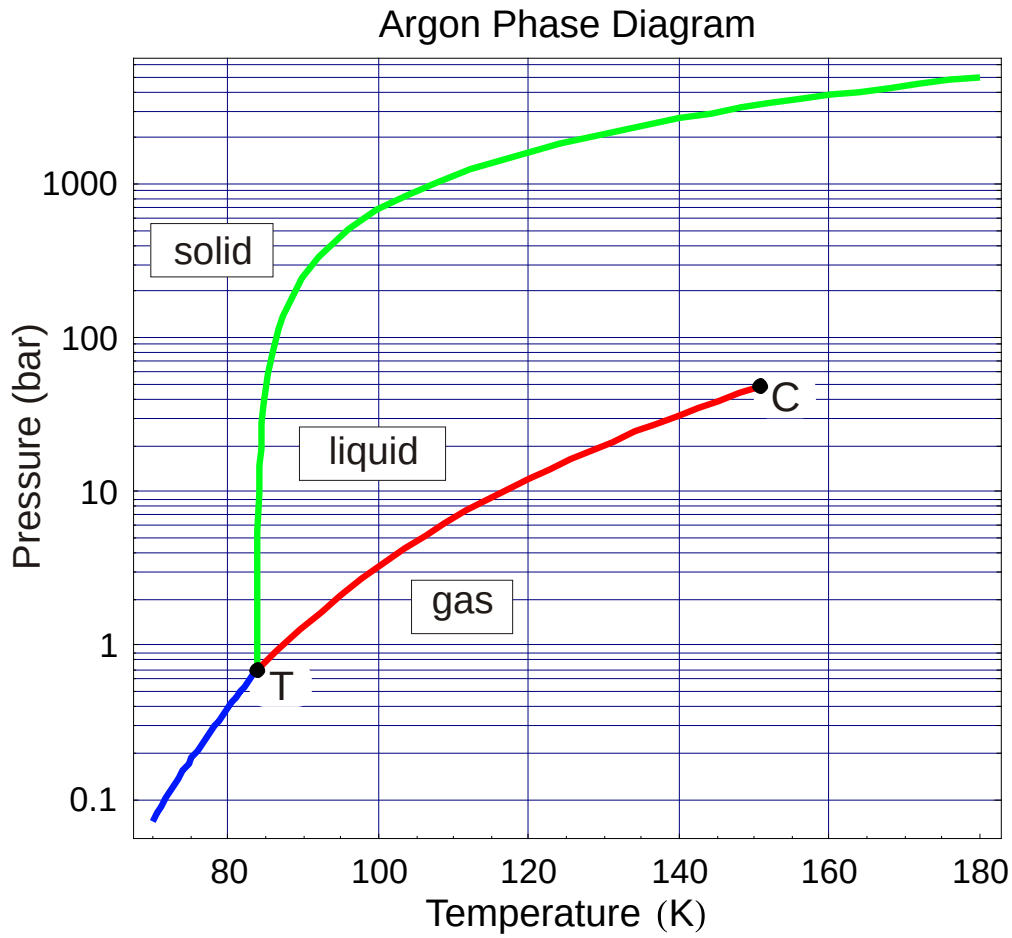

Enthalpy

Fit to enthalpy data from [5]

Pade approximant:

$$\Delta H = \frac{A + BT}{1 + CT}$$

ΔH = enthalpy of vaporization in kJ/mol

T = temperature in K

for 83.8 $\leq T \leq$ 100, $A = 7.98304$, $B = -0.0481275$, $C = -0.0047259$

RMS deviation = 0.167 J/mol

Vapor Pressure [5]

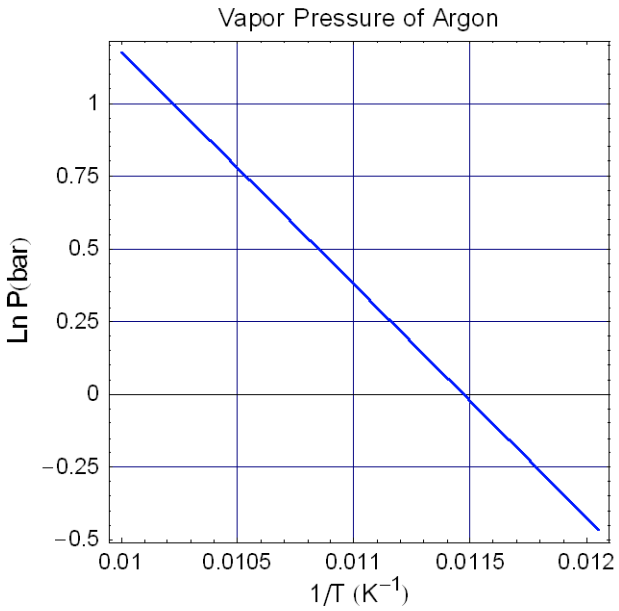

Modified Clausius-Clapeyron Equation:

$$\ln\frac{P}{P_C}=\frac{T_C}{T}(At+Bt^{1.5}+Ct^2+Dt^{4.5})$$

$t=(1-T/T_C)$

P = vapor pressure in bar

T = temperature in K

$T_C,\ P_C$ = $150.687K, 48.63\ bar$

for $T_T \le T \le T_C$, $A=-5.940\,978\,5$, $B=1.355\,388\,8$, $C=-0.464\,976\,07$ $D=-1.539\,904\,3$

Density [5]

Polynomial approximant:

$$\ln\frac{\rho_{LIQUID}}{\rho_C}=At^{0.334}+Bt^{2/3}+Ct^{7/3}+Dt^4$$

$t=(1-T/T_C)$

ρ_{LIQUID} = density in g/cm^3

T = temperature in K

$T_C, \rho_C = 150.687K, 0.5356$ g/cm^3

for $T_T \le T \le T_C$, $A=1.500\,426\,2$, $B=-0.313\,812\,90$, $C=0.086\,461\,622$ $D=-0.041\,477\,525$

Dielectric constant [6, 7]

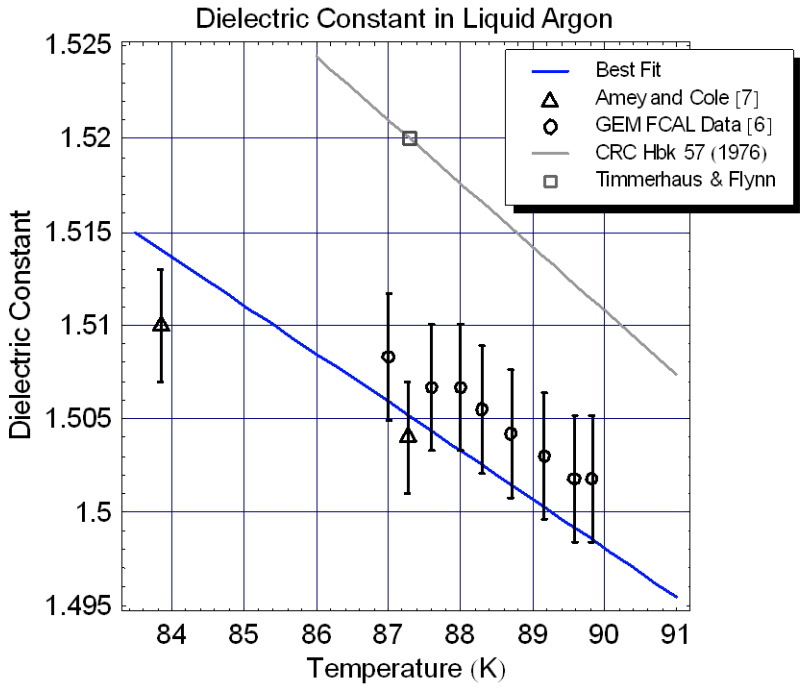

Data are points from:

[Circles] W. Don Carlos, et al., *Experimental data on GEM LAC FCAL tube design*, GEM TN-92-179 (1992) (unpublished).

[Triangles] R.L. Amey and R.H. Cole, *Dielectric constants of liquefied noble gases and methane*, J. Chem. Phys. **40** (1964) 146.

[Gray line] The Handbook of Chemistry and Physics, 57th edition, CRC Press (1976). Page E-55 gives the value of $1.53_8$for the value of the dielectric constant at 82.15K, with a linear temperature slope of $-0.34 \times 10^{-4}\ K^{-1}$.

[Gray square] K.D. Timmerhaus and T.M. Flynn, Cryogenic Process Engineering, Plenum Press NY (1989), p20 gives κ=1.52 at the normal boiling point.

Clausius-Mossotti relation:

$$\kappa = \frac{1+2\alpha_{CM}\rho_L}{1-\alpha_{CM}\rho_L}$$

κ = dielectric constant of the liquid

ρ_L = liquid density (see density section above)

with $\alpha_{CM} = 0.1033\ \mathrm{cm}^3/\mathrm{gm}$

for $T_T < T < T_C$

Index of refraction [8, 9, 10]

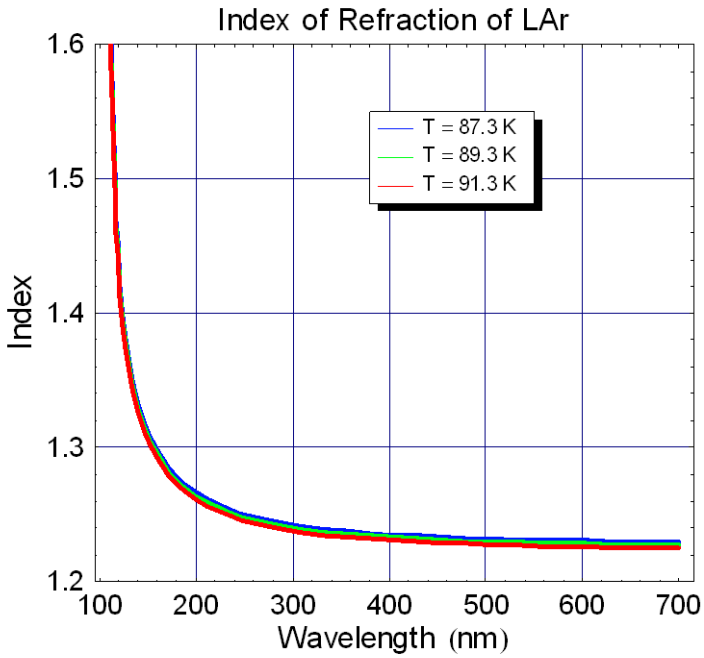

Lorentz-Lorentz relation:

$$n_L = \sqrt{\frac{\frac{\rho_G}{\rho_L}(n_G^2+2)+2(n_G^2-1)}{\frac{\rho_G}{\rho_L}(n_G^2+2)-(n_G^2-1)}}$$

$$n_G = 1 + c\left(\frac{a1}{b1-\lambda^{-2}} + \frac{a2}{b2-\lambda^{-2}} + \frac{a3}{b3-\lambda^{-2}}\right)$$

n_L = index of refraction of the liquid at λ (μm)

ρ_G = gas density = 0.001790 gm/cm^3

ρ_L = liquid density (see density section above)

with $c = 1.2055\times10^{-2}$

$a1 = 0.2075$ $\quad a2 = 0.0415$ $\quad a3 = 4.333$

$b1 = 91.012\,\mu\text{m}^{-2}$ $\quad b2 = 87.892\,\mu\text{m}^{-2}$ $\quad b3 = 214.02\,\mu\text{m}^{-2}$

for $T_T < T < T_C$

Rayleigh scattering attenuation length [11, 12, 13]

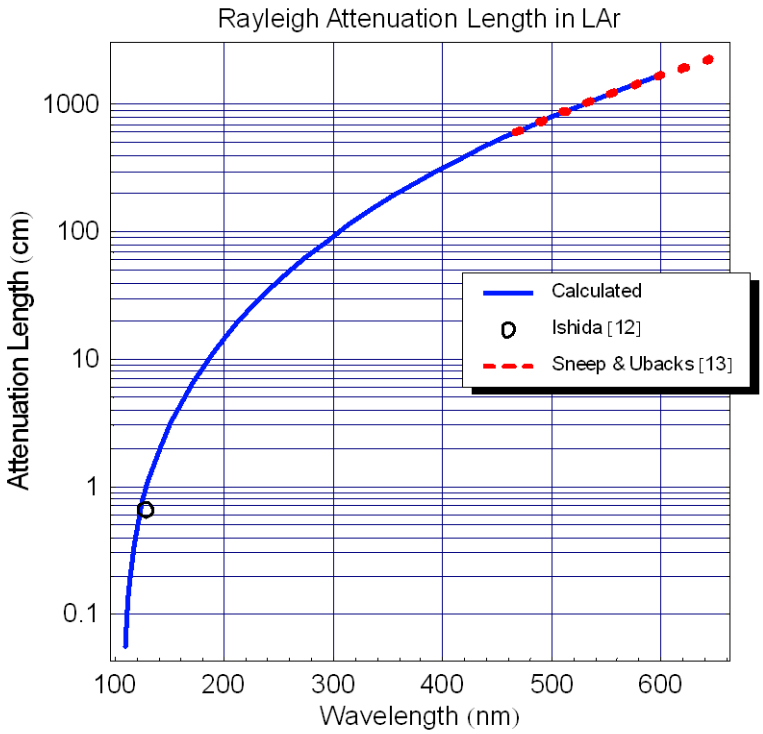

$$L_R^{-1} = \frac{k_B T \rho(T)^2 \kappa_T}{96\pi^5 \lambda^4} \left(\frac{(\epsilon(\lambda)-1)(\epsilon(\lambda)+2)}{3\rho(T)} \right)^2$$

L_R = Rayleigh scattering attenuation length

$\epsilon(\lambda)$ = dielectric constant at wavelength $\lambda = n(\lambda)^2$

$\rho(T)$ = density at temperature T

κ_T = isothermal compressibility = 2.18×10^{-10} cm^2/dyne

If the difference in the attenuation lengths calculated for Rayleigh scattering (94 cm) and measured by Ishida (66±3)[12] can be attributed to atomic absorption in the measurement, then the partial attenuation length for atomic absorption in their experiment is ~ 2 m. Absorption by atomic Ar is very small at 128 nm; the nearest resonance transition is at 106.7 nm. The absorption length determined from the dispersion, for a reasonable line width, via the Kramers-Kroenig dispersion relation is >1000 m at 128 nm. Absorption by impurities (O_2, N_2, H_2O and carbon compounds) is probably the dominant absorptive mechanism in LAr at 128 nm. The cross section for absorption by O_2 at 128 nm is about 3×10^{-19} cm^2 [40], which implies an attenuation length of 2.1 m for 800 ppb O_2 in LAr. The cross section for N_2 is about 1.2×10^{-18} cm^2 [41] so an N_2 concentration of 170 ppb contributes 2.1 m to the total absorption length. H_2O may be the dominant contributor: the cross section at 128 nm is 7.4×10^{-18} cm^2 [42] for an attenuation length of 2.1 m for 30 ppb.

Electron drift velocity [22, 23, 24, 25]

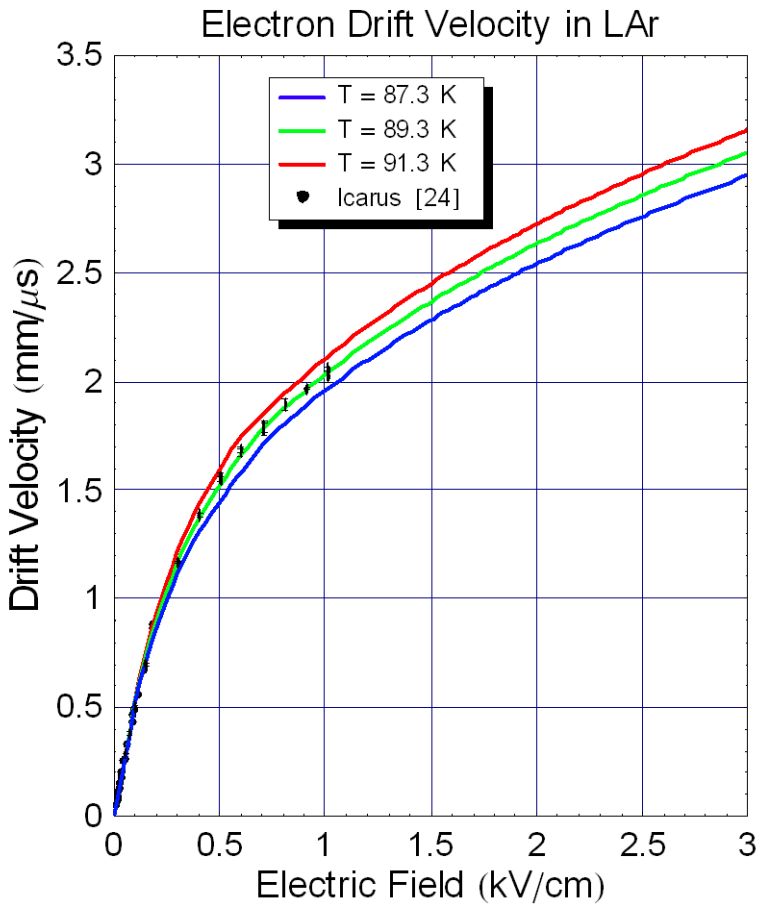

Kalinin empirical function[22] fit to Icarus[24] and Aprile[25] data:

$$v_{e^-,DRIFT} = (1 + p1(T - t0)) \times (p3\,E\,Ln[1 + p4/E] + p5\,f^{p6}) + p2(T - t0)$$

$v_{e^-,DRIFT}$ = electron drift velocity in mm/μs

T = temperature in K

E = electric field in kV/cm

valid for $87 \le T \le 94$ *and* $0.3 \le E \le 0.8$

$p1 = -0.0462553$ p2=0.0148508 $p3 = 1.64156$ $p4 = 1.273$

$p5 = 0.0086608$ $p6 = 4.71489$ $t0 = 104.326$

Curves in the figure are this parameterization below 0.7 kV/cm, merging smoothly (continuous derivative) with Walkowiak [23] parameterization above 0.8 kV/cm.

Electron diffusion [27, 28, 29, 30]

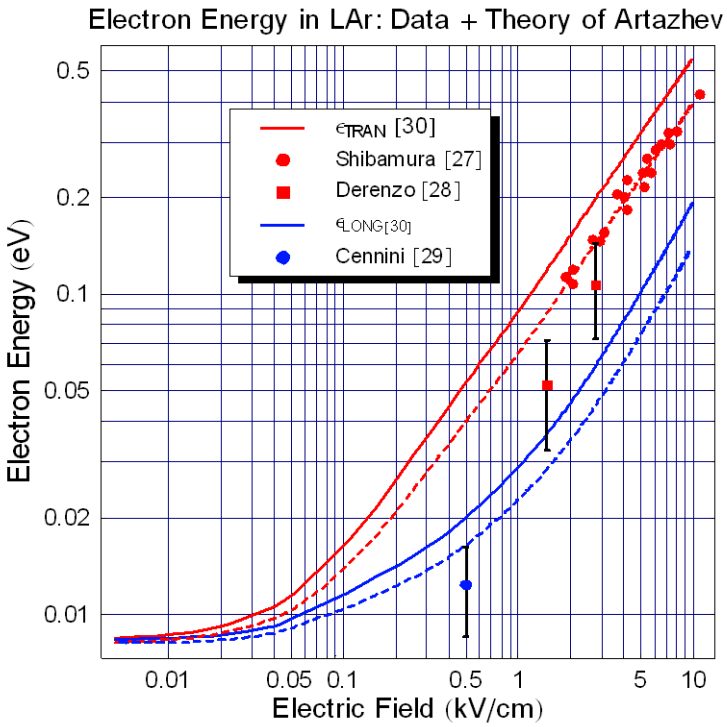

The data for transverse diffusion come from [27, 28]. The longitudinal diffusion is a single measurement from [29]. The transport theory calculation (solid lines) is from Atrazhev and Timoshkin [30], interpolated to the normal boiling point. We plot the electron energy, ε, rather than the diffusion coefficient, D, because the electron energy is the quantity directly measured by experiment (for longitudinal diffusion at least) and is the quantity directly entering in the calculation of the RMS spatial spread of an ensemble of electrons:

$$\sigma_{T(L)} = \sqrt{\frac{2\,\varepsilon_{T(L)}\,\Delta z}{E}}$$

with Δz the drift distance and E the field in volts per unit of drift distance. The Einstein-Smoulchowski relation defines the diffusion constant in terms of the electron energy:

$$D = \mu\,\varepsilon\,,$$

so that the diffusion constant requires the additional knowledge of the electron mobility μ. The dashed lines are the Atrazhev and Timoshkin theory scaled to the transverse data which give ε_{TRAN} = 40 meV (D_{TRAN} = 12.8 cm^2/s) and ε_{LONG} = 16.5 meV (D_{LONG} = 5.3 cm^2/s) at 500 V/cm.

Ion Drift Velocity [26]

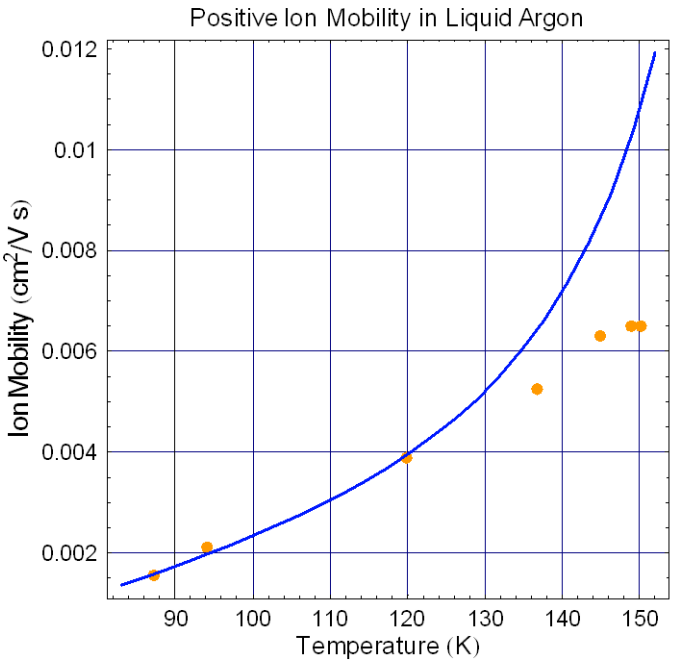

Gee, *et al*. [26] provide measurements of the positive ion mobility in liquid argon from the normal boiling point up to the critical point, and demonstrates that the mobility is independent of electric field and that the product of mobility and liquid viscosity are constant (Stoke's law):

$$\mu_+ \eta = (4.3 \pm 0.3) \times 10^{-6}\ Poise\, cm^2 / V s$$
$$\text{for } 87.2\text{K} \le \text{T} \le 135\text{K}$$

The curve in the figure above is the liquid viscosity from [5] scaled to the lowest three data points of [26].

Pade approximant:

$$\eta(T) = \frac{A + BT^{-1} + CT^{-2}}{1 + DT^{-1} + ET^{-2}}$$

$$v_{D,Ion}(E,T) = 4.32 \times 10^{-6}\, E\, \eta(T)$$

$v_{D,Ion}$ = positive ion drift velocity in mm/μs

T = temperature in K

E = electric field in V/cm

$$for\ 83.8 \le T \le 100, \quad A = -2.46184 \times 10^{8}, \quad B = 4.51273 \times 10^{10}, \quad C = -4.51527 \times 10^{11},$$
$$D = 2.15074 \times 10^{8}, \quad E = -1.28168 \times 10^{10}$$

Ions are in thermal equilibrium with the liquid, so the diffusion coefficient is

$$D_+ = \mu_+ \eta \times k_B T_{NBP} = 3.2 \times 10^{-3} cm^2 / s$$

Recombination [31, 32, 43]

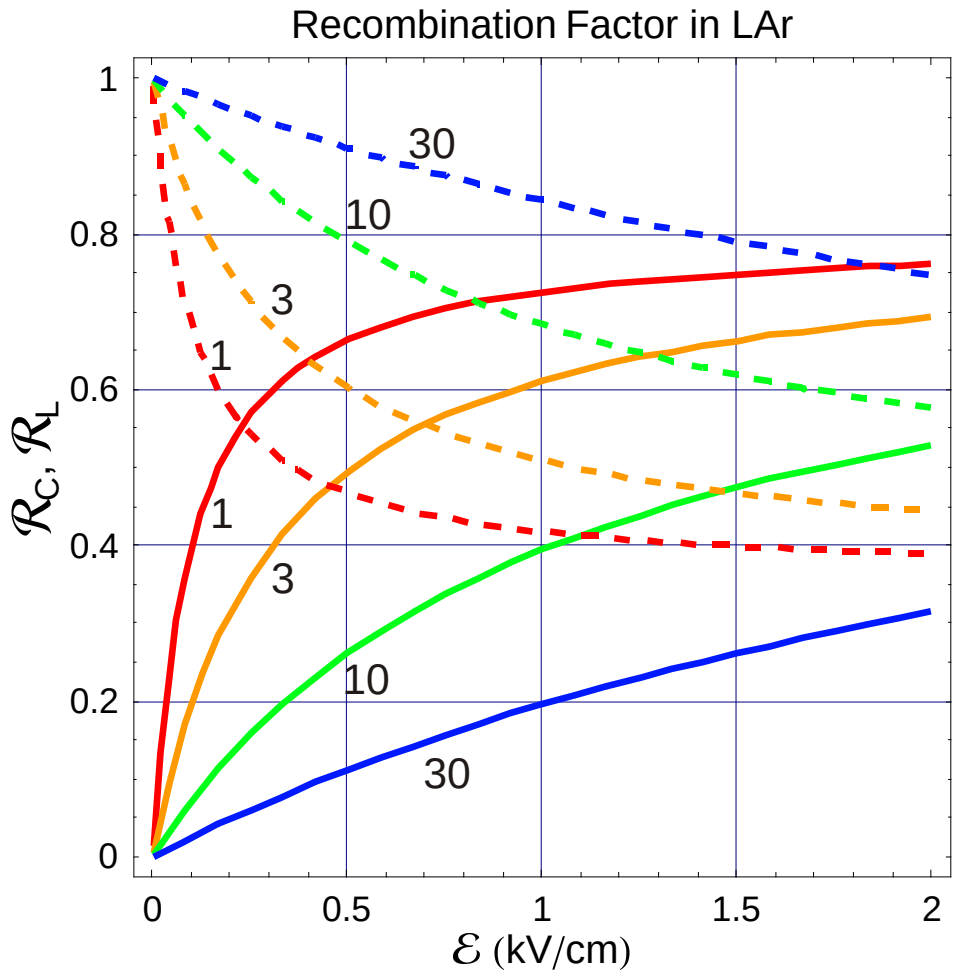

Solid lines are the recombination factor for charge (charge collected at finite field divided by charge collected at infinite field) [31, 32]. Dashed lines are the light recombination factor (light collected at field divided by light collected at zero field) [43]. The numbers labeling the curves are the specific energy loss (dE/dx) in units of mip.

$$R_C = \frac{Q}{Q_\infty} = \frac{A}{1 + \frac{k}{\mathcal{E}} \times \frac{dE}{dx}}$$

$$R_L = \frac{L}{L_0} = 1 - \alpha R_C$$

$\mathcal{E}$ *is electric field in kV / cm*

dE/dx is specific energy loss in MeV cm^2/g

with A=0.800, α=0.803, and k=0.0486 (kV/cm)/(MeV cm^2/g)

for $0.1 < \mathcal{E} < 1.0$ *kV / cm and* $1.5 < \mathrm{dE}/\mathrm{dx} < 30$ *MeV* cm^2 / *g*

Electron attachment [33, 34, 35, 36]

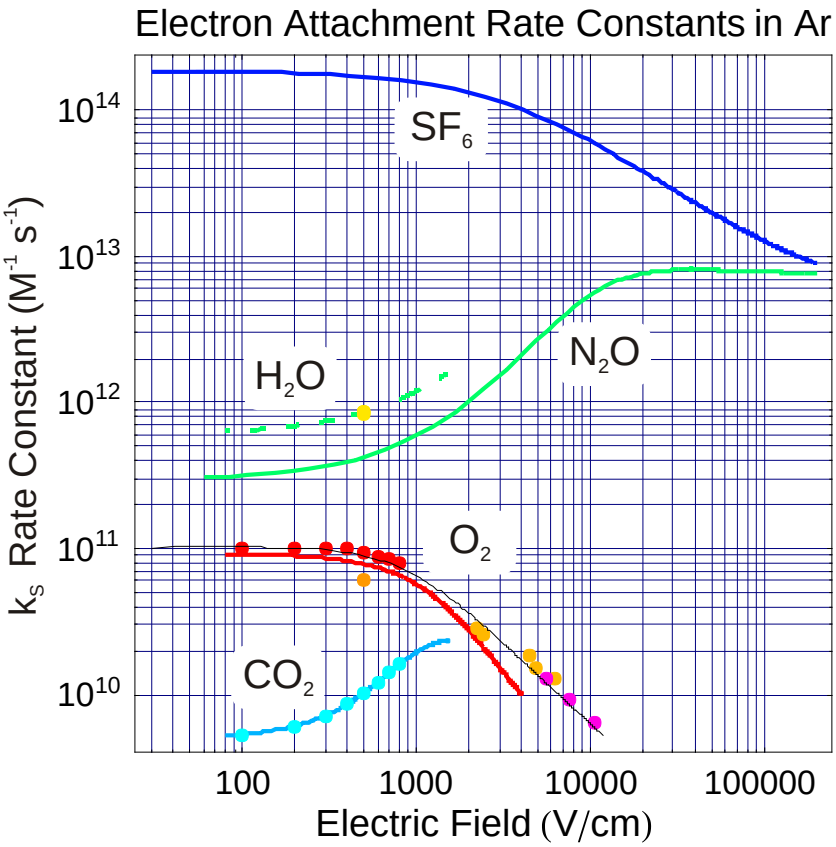

The solid lines for O_2, N_2O, and SF_6 are from Bakale, Sowada, and Schmidt [33]; the red points for O_2 and all the points for CO_2 are from Bettini (ICARUS) [34]; for O_2 the orange points are from Aprile, Giboni, and Rubbia [35] (at 500 V/cm) and from Adams, *et al*. [36] (for the points above 2kV/cm), and the magenta points are from Hofmann, et al. [37]; and the yellow point for H_2O is from μBooNE docDB 429-v1 and the dashed curve is the curve for N_2O scaled to this point. The solid black line is a best fit, specified below, to the data for O_2.

$$Q(t) = Q_0\, Exp(-t/\tau_A)$$

with $\tau_A = (k_S\, n_S)^{-1}$

k_S is electron attachment rate constant in $M^{-1}\, s^{-1}$

n_S is molar (M) solute concetration in LAr

$1\ \mathrm{M} = 2.503\times10^{-8}\, \rho_{LIQUID}(T)\times \mathrm{ppb}$

the attachment rate constant depends on electric field

$$k_S = \frac{p_0 + p_1 E + p_2 E^2}{1 + q_1 E + q_2 E^2 + q_3 E^3}$$

with $p_0 = 348.066$ $p_1 = 44068.9$ $p_2 = 27.3268$

$q_1 = 4351.98$ $q_2 = 1.88415$ $q_3 = 0.00478478$

E *is in* V/cm

Breakdown Voltage [44, 45, 46]

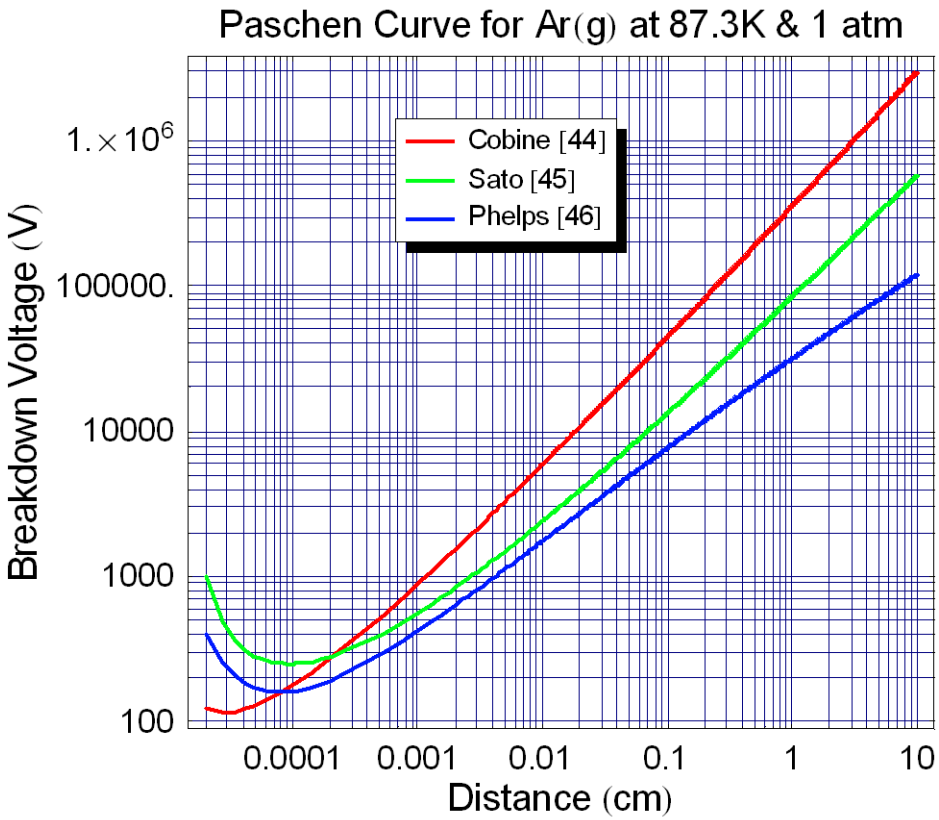

All of the curves in the figure are scaled from measurements made at and above room temperature. This requires an extrapolation to reach the largest distances in the figure. The "Phelps" curve represents actual measurements up to 1 cm on this scale; the others are larger extrapolations. The breakdown voltage is very sensitive to the presence of electronegative impurities at large distances, and to electrode preparation at small distances. Electronegative impurities and dirty electrodes increase the breakdown voltage. Since the cleanliness of LAr is extremely good, it is advisable to assume that actual breakdown will occur below the lowest reported values in gas at higher temperatures.

References

1. P. Benetti, *et al.*, *Measurement of the specific activity of ^{39}Ar in natural argon*, NIM **A574** (2007) 83.

2. V.D. Ashitkov, *et al.*, *New experimental limit on the ^{42}Ar content in the Earth's atmosphere*, NIM **A416** (1998) 179.

3. Table of the Isotopes, LBNL Isotopes Project (http://ie.lbl.gov/toi/)

4. Ch. Tegler, R. Span, and W. Wagner, *A new equation of state for argon covering the fluid region for temperatures from the melting line to 700K at pressures up to 1000MPa*, J. Phys. Chem. Ref. Data, **28** (1999) 779.

5. "Thermophysical Properties of Fluid Systems" by E.W. Lemmon, M.O. McLinden and D.G. Friend in **NIST Chemistry WebBook, NIST Standard Reference Database Number 69**, Eds. P.J. Linstrom and W.G. Mallard", National Institute of Standards and Technology, Gaithersburg MD, 20899, http://webbook.nist.gov/chemistry/fluid/, (retrieved April 30, 2009).

6. W. Don Carlos, *et al.*, *Data on GEM LAC FCAL tube design*, JGEM TN-92-179 (1992) (unpublished).

7. R.L. Amey and R.H. Cole, *Dielectric constants of liquefied noble gases and methane*, J. Chem. Phys. **40** (1964) 146.

8. R.K.Teague and C.J. Pinge, *Refractive index and the Lorentz-Lorentz function for gaseous and liquid argon, including a study of the coexistence curve near the critical state*, J. Chem. Phys. **48** (1968) 4973.

9. R.A. Bideau-Mehu, Y. Guern, R. Abjean, and A. Johannin-Gilles, *Measurement of refractive indices of neon, argon, krypton and xenon in the 253.7-140.4 nm wavelength range: dispersion relations and estimated oscillator strengths of the resonance lines*, J. Quant. Spectrosc. Ratiat. Transfer **25** (1981) 395.

10. A.C. Sinnock and B.L. Smith, *Refractive indices of the condensed inert gases*, PR **181** (1969) 1297.

11. G.M. Seidel, R.E. Lanou, and W. Yao, *Rayleigh scattering in rare-gas liquids*, NIM **A489** (2002) 189.

12. N. Ishida, *et al.*, *Attenuation length measurements of scintillation light in liquid rare gases and their mixtures using an improved reflection suppresser*, NIM **A384** (1997) 380.

13. M. Sneep and W. Ubachs, *Direct measurement of the Rayleigh scattering cross section in various gasses*, J. Quant. Spectrosc. Radiat. Transf. **92** (2005) 293.

14. M.E. Shibamura, *et al.*, *Drift velocities of electrons, saturation characteristics of ionization and W-values for conversion electrons in liquid argon, liquid argon-gas mixtures and liquid xenon*, NIM **131** (1975) 249.

15. M.Miyajima, *et al.*, *Average energy expended per ion pair in liquid argon, liquid argon-gas mixtures and liquid xenon*, Phys. Rev. **A9** (1974) 1438, and erratum in **A10** (1974) 1452.

16. T. Doke, *et al*., *Absolute scintillation yields in liquid argon and xenon for various particles*, Jpn. J. Appl. Phys. **41** (2002) 1538.

17. M. Antonello, *et al.*, *Detection of Cherenkov light emission in liquid argon*, NIM **A516** (2004) 348.

18. T. Doke, *et al*., *Estimation of Fano factors in liquid argon, krypton, xenon, and xenon-doped liquid argon*, J. Appl. Phys. **57** (1985) 1097.

19. C. Amsler, *et al., 2008 Review of Particle Physics*, Phys. Lett. **B667** (2008) 1 (http://pdg.lbl.gov/2008/reviews/rpp2008-rev-passage-particles-matter.pdf).

20. M.G. Boulay and A. Hime, *Technique for direct detection of weakly interacting massive particles using scintillation time discrimination in liquid argon*, Astropart. Phys. **25** (2006) 179.

21. A. Hitachi, *et al*., *Effect of ionization density on the time dependence of luminescence from liquid argon and xenon*, Phys. Rev. **B27** (1983) 5279.

22. A.M. Kalinin, Yu.K. Potrebennikov, A. Gonidec, and D. Schinzel, *Temperature and electric field strength dependence of electron drift velocity in liquid argon*, ATLAS Internal Note LARG-NO-058 (1996).

23. W. Walkowiak, *Drift velocity of free electrons in liquid argon*, NIM **A449** (2000) 288.

24. S. Amoruso, *et al*., *Analysis of the liquid argon purity in the ICARUS T600 TPC*, NIM **A516** (2004) 68.

25. E. Aprile, K.L. Gibone, and C. Rubbia, *A study of ionization electrons drifting large distances in liquid and solid argon*, NIM **A241** (1985) 62.

26. N. Gee, *et al*., *Ion and electron mobilities in cryogenic liquids: argon, nitrogen, methane, and ethane*, J. Appl. Phys. **57** (1985) 1097.

27. ME. Shibamura, *et al*., *Ratio of diffusion coefficient to mobility for electrons in liquid argon*, Phys. Rev. **A20** (1979) 2547.

28. S. DeRenzo, *Electron diffusion and positive ion charge retention in liquid-filled high-resolution multi-strip ionization-mode chambers*, Lawrence Berkeley Laboratory, Group A Physics Note No. 786 (1974).

29. P. Cennini, et al., *Performance of a three-ton liquid argon time projection chamber*, NIM **A345** (1994) 230.

30. Atrazhev, V.M. and I.V. Timoshkin, *Transport of electrons in atomic liquids in high electric fields*, IEEE Trans. Dielectrics and Electrical Insulation **5** (1998) 450.

31. J. Thomas and D.A. Imel, *Recombination of electron-ion pairs in liquid argon and liquid xenon*, Phys. Rev. **A36** (1987) 614.

32. S. Amoruso, *et al*., *Study of electron recombination in liquid argon with the ICARUS TPC*, NIM **A523** (2004) 275.

33. G. Bakale, U. Sowada, and W.F. Schmidt, *Effect of electric field on electron attachment to SF_6, N_2O, and $_{O2}$ in liquid argon and xenon*, J. Phys. Chem. **80** (1976) 2556.

34. A. Bettini, *et al.*, *A study of the factors affecting the electron lifetime in ultra pure liquid argon*, NIM **A305** (1991) 177.

35. E. Aprile, K.L. Giboni, and C. Rubbia, *A study of ionization electrons drifting large distances in liquid and solid argon*, NIM **A241** (1985) 62.

36. M. Adams, *et al*., *A purity monitoring system for liquid argon calorimeters*, NIM **A545** (2005) 613.

37. W. Hofmann, *et al*., *Production and transport of conduction electrons in a liquid argon ionization chamber*, NIM. **135** (1976) 151.

38. E. Trakhovsky, *et al*., *Contribution of oxygen to attenuation in the solar blind UV spectral region*, App. Opt. **28** (1989) 1588.

39. K. Yoshino, *et al*., *Effect of molecular solutes on the electron drift velocity in liquid Ar, Kr, and Xe*, Phys. Rev. **A14** (1976) 438.

40. R. Goldstein and F.N. Mastrup, *Absorption coefficients of the O_2 Schumann-Runge continuum from 1270 A to 1745 A using a new continuum source*, J. Opt. Soc. Am. **56** (1966) 765.

41. G.L. Weissler, P. Lee, and E.I. Mohr, *Absolute absorption coefficients of nitrogen in the vacuum ultraviolet*, J. Opt. Soc. America, **42** (1952) 84.

42. K. Watanabe and M. Zeilikoff, *Absorption coefficients of water vapor in the vacuum ultraviolet*, J. Opt. Soc. Am. **43** (1953) 753.

43. S. Kubota, *et al*., *Recombination luminescence in liquid argon and in liquid xenon*, Phys. Rev. **B17** (1978) 2762.

44. J. Cobine, Gaseous conductors, Dover, NY (1958).

45. M. Sato, *Interpretation for argon breakdown in DC and microwave fields*, Bull. Yamagata Univ. **25** (1999) 119.

46. A.V. Phelps and Z.Lj. Petrovic, *Cold-cathode discharges and breakdown in argon: surface and gas phase production of secondary electrons*, Plasma Sources Sci. Technol. **8** (1999) R21.